Supplementary Material for
Modeling of Atomic Layer Etching of SiO_2 Using HF/NH_3 Co-Dosing

This document provides model formulation details, validation data, and supplementary figures supporting the abstract. The reaction schemes relevant to the plasmaless COR process and considered in the present model are:

$$\begin{aligned} SiO_2(s) + 4\,HF(g) &\longrightarrow SiF_4(g) + 2\,H_2O(g) \\ SiO_2(s) + 4\,HF(g) + 4\,NH_3(g) &\longrightarrow SiF_4(g) + 2\,H_2O(g) + 4\,NH_3(g) \\ SiF_4(g) + 2\,HF(g) + 2\,NH_3(g) &\longrightarrow (NH_4)_2SiF_6(s) \end{aligned} \tag{1}$$

The COR ALE model is formulated as a parallel-resistance reaction rate framework that accounts for both surface-limited reaction rates and diffusion-limitted reaction rates through the modified AFS layer. The total reaction rate is expressed as the inverse sum of individual surface rate contributions, allowing multiple chemically viable pathways (Eq. 1) to act concurrently.

$$\frac{1}{R_{total}} = \frac{1}{R} + \sum_i \frac{1}{R_i} \tag{2}$$

$$R = k \sum_i c_i C_{g,i} \tag{3}$$

$$R_i = \frac{c_i h_{crit} D_i (C_{g,i} - C_{int,i})}{h^2} \tag{4}$$

$C_{g,i}$ are the respective precursor concentrations in the gas phase and $C_{int,i}$ are the concentrations at the interface which are assumed to be zero due to instantaneous reaction and therefore consumption. k is the rate on the bare surface, c_i are the stoichiometric factors, D_i the diffusion coefficients through AFS, h_{crit} the nominal height at which we assume surface coverage and h the thickness of the AFS layer. The first term (Eq. 3) in Eq. 2 refers to the reaction pathway, where both precursors are available on the uncovered SiO_2 surface and form AFS. The next two terms (Eq. 4) capture the diffusion limited regime, where precursors are reaching the surface due to a concentration gradient and are modeled following a $1/h^2$ dependence on the thickness of AFS.
$R_{total}(h)$ is then used as the total rate of AFS formation to calculate the thickness h of the AFS layer, while the contribution from volatile etching is accumulated as $R_{etch}(h)$ with constant rate r_{etch}.

$$\frac{dh}{dt} = \frac{m_{AFS}}{\rho_{AFS}} R_{total}(h) \tag{5}$$

$$\frac{de}{dt} = \frac{m_{SiO_2}}{\rho_{SiO_2}} R_{etch}(h) \tag{6}$$

$$R_{etch}(h) = \frac{1}{2}\left[1 - \tanh\left(\frac{h - h_{crit}}{\delta}\right)\right] r_{etch} \tag{7}$$

The thickness dependent coverage function in Eq. 7 allows this pathway only to occur in regions where the surface is treated as bare. The parameters h_{crit} and δ allow for tuning of this behavior and are chosen to start passivating the surface only after monolayer thickness is reached.

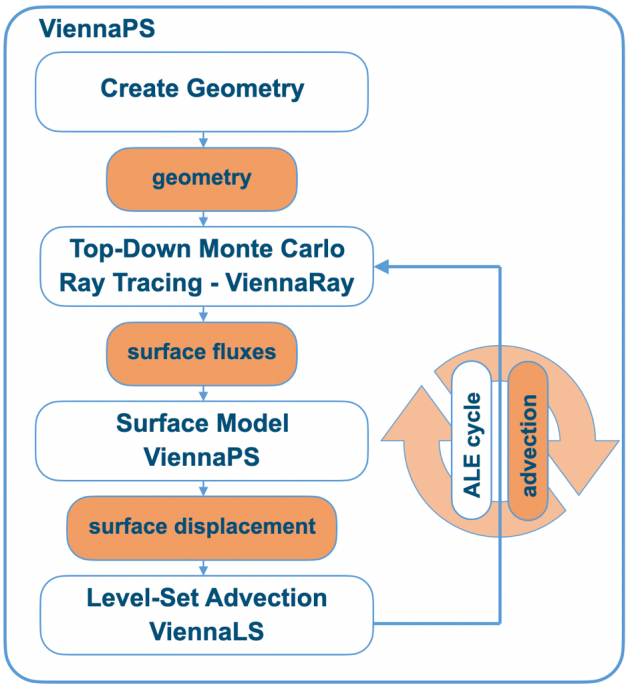

FIG. 1. Schematic of the feature-scale ALE model as implemented in ViennaPS [1]. Gas-phase precursor transport is simulated using top down Monte Carlo ray tracing on the geometry, yielding local surface fluxes. These are used in the surface model to obtain the precursor surface concentrations. AFS formation is modeled as described in Eq. 2- 4 via surface-limited reactions and diffusion-limited reactions . Direct volatile etching of SiO_2 by HF becomes active under conditions of incomplete surface coverage as described in Eq. 7. The thus obtained surface displacement Eq. 8 is then used to propagate the surface using the level-set method as provided by ViennaLS. This completes one ALE cycle. In the adaptive scheme employing the cycle-skipping strategy, this advection is performed multiple times before the surfaces fluxes are recalculated in the ray tracing step.

Both surface rates are integrated over the reactant-pulse time to yield the associated displacements D_{AFS} and D_{etch}, where 31% of the AFS thickness is removed according to the mass-density ratio of SiO_2 and AFS. The thus obtained combined surface displacement d_t is then used to propagate the surface with the level-set method.

$$d_t = D_{AFS} + D_{etch} = 0.31 \cdot \int_0^t \frac{dh}{dt'} dt' + \int_0^t \frac{de}{dt'} dt' \tag{8}$$

Runtimes (Tab.I) scale approximately with the number of flux recalculations, as the computational cost of surface displacement evaluation dominates over the cost of surface advection using the level-set method.

[1] T. Reiter and L. Filipovic, "Viennaps: A flexible framework for semiconductor process simulation," SoftwareX **32**, 102453 (2025).
[2] Y. Hagimoto, H. Ugajin, D. Miyakoshi, H. Iwamoto, Y. Muraki, and T. Orii, "Evaluation of the plasmaless gaseous etching process," in *Ultra Clean Processing of Semiconductor Surfaces VIII*, Solid State Phenomena, Vol. 134 (Trans Tech Publications Ltd, 2008) pp. 7–10.

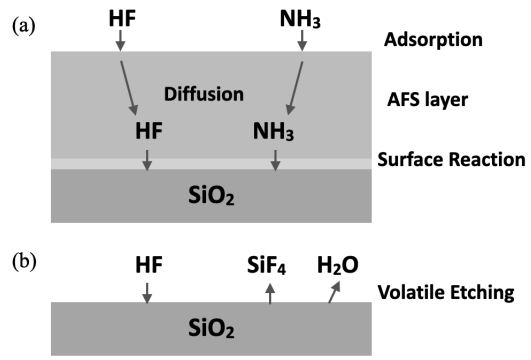

FIG. 2. Schematic of viable reaction pathways according to the plasmaless COR chemistry in Eq.1. (a) Pathway showing AFS formation by diffusion of precursors. (b) Direct volatile etching of SiO_2 by HF.

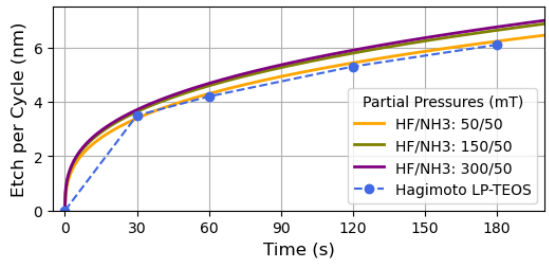

FIG. 3. Evolution of AFS thickness during cyclic HF/NH_3 ALE of SiO_2. Solid lines show model predictions for different precursor partial pressures, while experimental thickness data reported by Hagimoto et al.[2] is shown dashed. The model captures both the transient and saturation behavior across the investigated pulse conditions.

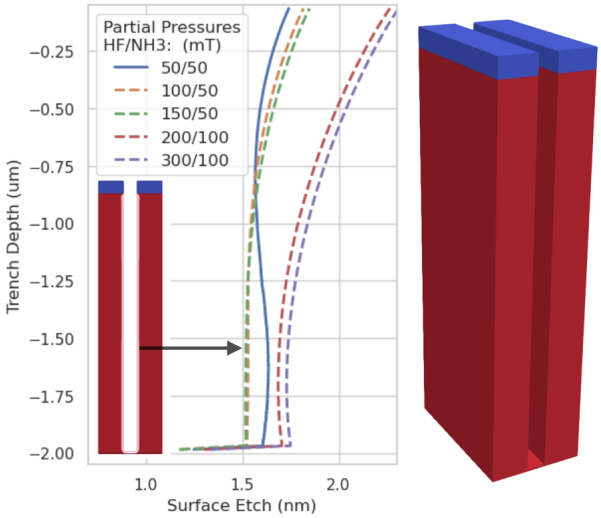

FIG. 4. Etch profiles for different HF/NH_3 co-dosing conditions in a HAR trench (AR = 20). Each curve corresponds to a combination of absolute HF and NH_3 partial pressures, as indicated in the legend. Variations in total precursor pressure and relative dosing ratio affect the growth of AFS and the resulting etch profile. Conditions closer to the stoichiometric ideal ($HF:NH_3$ = 3:1) yield higher conformality due to faster growth and prohibited volatile etching (dashed green, orange). Higher partial pressures lead to higher overall etch depths (dashed red, violet). Under specific conditions inverse aspect ratio dependent etching can occur (solid blue at 1.5 μm depth) meaning the surface etch is higher in the bottom than at the top of the trench.

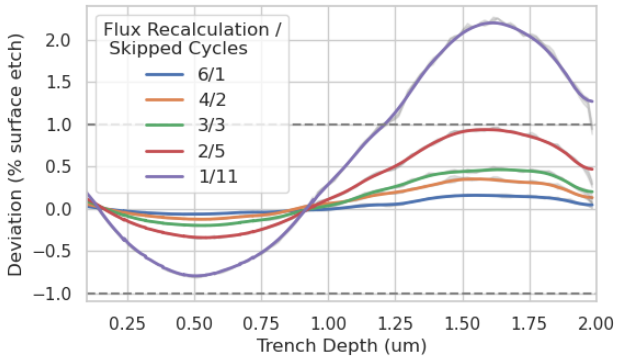

FIG. 5. Deviation of etched surface profiles from gauge simulations as a function of trench depth for different flux-recalculation strategies. Labels indicate the number of explicit flux evaluations followed by the number of skipped ALE cycles. All profiles are simulated for a total of twelve ALE cycles. Deviations from the gauge profile remain below $\pm 1\%$ for up to 5 skipped cycles (solid red).

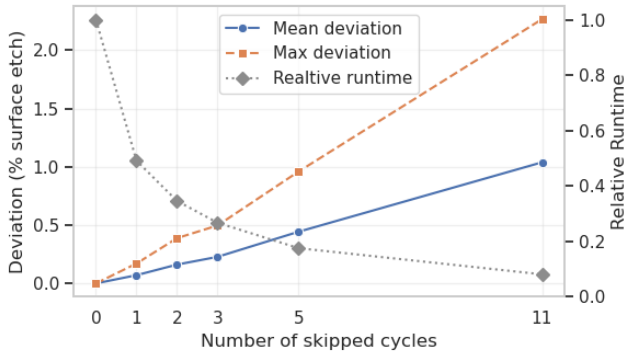

FIG. 6. Mean (blue) and maximum (orange) deviations for different flux-recalculation strategies. Computational efficiency of different flux-recalculation strategies for a total of twelve ALE cycles shown in grey. Runtime and deviations are normalized to the gauge simulation with flux-recalculation for every ALE cycle.

TABLE I. Computational efficiency and mean deviation of different flux-recalculation strategies for a total of twelve ALE cycles. Runtimes and deviations are normalized to the gauge simulation (12/0) with flux-recalculation for every ALE cycle.

Recalculations / Skipped Cycles	Deviation	Relative Runtime
12/0 (Gauge)		1.0×
6/1	0.07 %	0.49×
4/2	0.16 %	0.35×
3/3	0.23 %	0.27×
2/5	0.44 %	0.17×
1/11	1.04 %	0.08×